RESEARCH

CrossMark

Investigating variations of the electron beam voltage on the traveling wave tube output power in the different frequencies

F. Sheykhe[1] · Sh. Saviz[1] · M. Salem[1]

Abstract

In the present research, the effect of variations of the electron beam voltage on the output power is studied. In order to develop the study, this problem was investigated at different frequencies, which are the products of nonlinear behavior of the traveling wave tube (TWT) in response to the input frequency. Moreover, for a more realistic understanding, the tubes were considered with two linear and nonlinear responses to the input frequency. The TWT output power was calculated in linear and nonlinear modes, at different frequencies using the numerical solution of the mathematical equations of the Lagrangian model. Then, the output power in terms of distance and beam voltage in different frequencies was plotted and compared. The results revealed that the effects of variations of voltage on the output power were more proper in a single-mode TWT in comparison with a multimode one.

Keywords Beam voltage · Output power · Nonlinear · Traveling wave tube

Introduction

Traveling wave tubes (TWTs) are devices that are widely used in communication, electronic warfare and radar systems [1, 2]. These devices have wide bandwidths, high-frequency and high-power operating points; as a result, they have wider spread application. The nonlinear behaviors of the TWTs are known as one of the important practical limits of them. Until now, many efforts have been made to reduce these nonlinear effects [7–9, 11, 12]. The nonlinearity features are recognized as spectral distortions and saturating mechanism [3]; both of which decrease the efficiency of the TWT.

For single-tone mode, nonlinear distortion products appear as harmonics products (f, $2f$, $3f…$), while for multi tone mode (multicarrier operation) nonlinear distortion products appear as intermodulation products (mf1 + nf2) at the output of the amplifier [3]. In this work, the effects of changes in beam voltage on the output power of TWTs are studied in both the presence and absence of a nonlinear phenomenon (spectral distortion).

The most important mechanism that occurs inside the tube is the interaction between the input wave and the electron beam. When an electron beam is injected along the axis of the helix, electric field horizontal component of the wave accelerates some electrons and decelerates the others. This is the basis for the formation of bunch of the electron beam and the transfer of energy from the beam to the wave and ultimately the amplification of the output wave [1, 2]. Electron beam emission voltage into the tube is the source of energy and beam velocity. Therefore, determination of the cathode voltage and its variations, which are the emitter of the electrons from the gun and called the beam voltage, is very important. In many previous attempts, the basis for selecting the voltage for the beam was the TWT efficiency and maximum output power. In the previous studies, the value of the beam voltage or the cathode voltage was equal to 3150 V [6, 10, 15]. In other studies, this value was considered as 2750 v in [11], 4350 v in [5], 4880 v in [13] and 4920 v in [14]. Therefore, in this study, the effects of voltage changes on the improvement in TWT output power is studied using numerical solution of the governing equations. The TWT is modeled by several authors using the Eulerian and Lagrangian electron beam coordinates [4].

✉ Sh. Saviz
   shahrooz.saviz@srbiau.ac.ir; azarabadegan@gmail.com

[1]   Plasma Physics Research Center, Science and Research
      Branch, Islamic Azad University, Tehran, Iran

Springer

Among all of the present models, the multi-frequency spectral Eulerian (MUSE) and Lagrangian TWT equations (LATTE) are the most important physical models. The basis of using these two models is the physical interpretation used for the electron beam as a fluid [4]. In "Formulation" section, we formulate the governing equations for the Lagrangian model of the TWT. The numerical solutions as well as the diagrams which show output power in terms of voltage and distance are presented in "Numerical results" section. Finally, the discussion and conclusion of the numerical results are given in "Discussion and Conclusion" section.

Formulation

The transmission line, Poisson, continuity and Vlasov equations are used to derive the mathematical equations of the TWT which are expressed in the domain of time as follows [3, 4, 16]:

Transmission line equations:

$$\frac{\partial V}{\partial z} = h_1 \frac{\partial I}{\partial t} \tag{1}$$

$$\frac{\partial I}{\partial z} = h_2 \frac{\partial V}{\partial t} - A \frac{\partial \rho}{\partial t} \tag{2}$$

In Eqs. (1) and (2), the current and voltage are expressed with I and V, respectively. The ρ, volume charge density, t, time and z is the axial distance.

Poisson's equation:

$$\frac{\partial E}{\partial z} = \frac{\rho}{\varepsilon_0} \tag{3}$$

In Eq. 3, E is the space charge electric field.

Continuity and Vlasov equations:

$$\frac{\partial v}{\partial t} + v\left(\frac{\partial v}{\partial z}\right) = -\frac{e}{m_e} h_1 \left(\frac{\partial I}{\partial t}\right) + \frac{e}{m_e} \Re E \tag{4}$$

$$\frac{\partial \rho}{\partial t} + v\left(\frac{\partial \rho}{\partial z}\right) = -\rho\left(\frac{\partial v}{\partial z}\right) \tag{5}$$

In Eqs. (1) and (2), the coefficients of and are the Fourier transforms inverse that are expressed as follows:

$$h_1(z,t) = F^{-1}\left\{\frac{\tilde{K}(z,f_l\omega_0)}{\tilde{v}_{\text{ph}}(z,f_l\omega_0)}\right\} \tag{6}$$

$$h_2(z,t) = F^{-1}\left\{\frac{1}{\tilde{v}(z,f_l\omega_0)\tilde{K}(z,f_l\omega_0)}\right\} \tag{7}$$

$$\Re(z,t) = F^{-1}\{\Re(z,f_l\omega_0)\} \tag{8}$$

where the functions $\tilde{v}_{\text{ph}}(z,f_l\omega_0)$, $\tilde{K}(z,f_l\omega_0)$ and $\Re(z,f_l\omega_0)$ are defined as cold circuit phase velocity, frequency

domain circuit interaction impedance and space charge reduction factor, respectively.

Using the furrier transform, Eqs. (1), (2), (3), (4) and (5) are transformed from the time domain to the frequency domain.

Using the coordinate transformation in Eqs. (9) and (10), where z is the distance and ψ is the phase. The phase is described with respect to a traveling wave of speed u_0 and frequency ω_0

$$z = z \tag{9}$$

$$\psi = \omega_0\left(\frac{z}{u_0} - t\right) \tag{10}$$

According to Fig. 1, in which, R is the resistance, C is capacitance, G is shunt, and L is the inductive series; applying Kirchhoff's voltage and current laws, Eqs. (1) and (2) are as follows.

$$\frac{\partial V}{\partial z} = RI - \frac{\omega_0}{u_0}\frac{\partial V}{\partial \psi} - \omega_0 L \frac{\partial I}{\partial \psi} \tag{11}$$

$$\frac{\partial I}{\partial z} = GV - \omega_0 C \frac{\partial V}{\partial \psi} - \frac{\omega_0}{u_0}\frac{\partial I}{\partial \psi} + A\omega_0 \frac{\partial \rho}{\partial \psi} \tag{12}$$

If Eqs. (9) and (10) are used, Eqs. (3), (4) and (5) are derived as follows.

$$\frac{\partial E}{\partial z} = -\frac{\omega_0}{u_0}\frac{\partial E}{\partial \psi} + \frac{\rho}{\varepsilon_0} \tag{13}$$

$$v\frac{\partial v}{\partial z} = \frac{e}{m_e}\left(\omega_0 L \frac{\partial I}{\partial \psi} - RI\right) + \frac{e}{m_e}\Re E + \omega_0\left(1 - \frac{v}{u_0}\right)\frac{\partial v}{\partial \psi} \tag{14}$$

$$v\frac{\partial \rho}{\partial z} = \omega_0\left(1 - \frac{v}{u_0}\right)\frac{\partial \rho}{\partial \psi} - \rho\left(\frac{\partial v}{\partial z} + \frac{\omega_0}{u_0}\frac{\partial v}{\partial \psi}\right) \tag{15}$$

In Eq. 14, v is the electron beam velocity and $\Re$ is space charge reduction factor.

Also, m_e and e are, respectively, the mass and the charge of the electron.
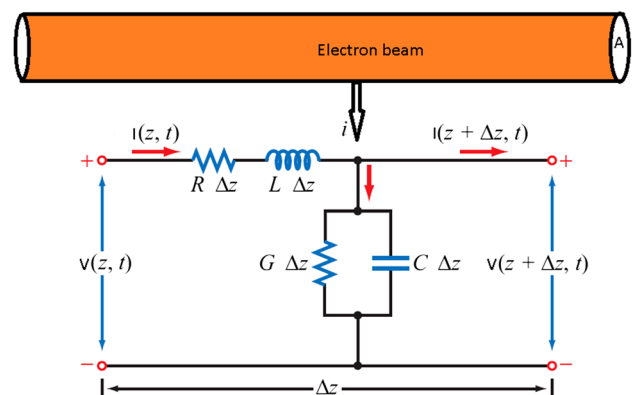

Fig. 1 Each section of the helix is represented by an equivalent circuit [16]

According to the above discussion, each TWT contains three main parts, the slow wave structure, the source of the electron beam and the propagation of an electromagnetic wave that have approximately the same phase velocity with electron beam. The mathematical Eqs. (11)–(15) form a differential equation system which describes the mechanism of the TWT. In order to normalize the quantities used, the following characteristic quantities are defined:

$$z = L \tag{16}$$

$$U = u_0 \tag{17}$$

$$T = \frac{z}{U} \tag{18}$$

In the above equations, u_0 is the DC beam velocity, L is the TWT circuit length, and T is a characteristic time. The following variables illustrate the normalization of dependent variables and independent coordinates [3, 4, 16].

Independent coordinates:

$$\hat{z} = \frac{z}{L} \tag{19}$$

$$\hat{\psi} = \frac{\psi}{\omega_0 T} = (\hat{z} - \hat{t}) \tag{20}$$

$$\hat{t} = \frac{t}{T}. \tag{21}$$

Dependent variables:

$$\tilde{V} = \frac{\mathbb{C}}{K I_0} V \tag{22}$$

$$\tilde{I} = \frac{\mathbb{C}}{I_0} I \tag{23}$$

$$\tilde{E} = \frac{\varepsilon_0}{L \rho_0} E \tag{24}$$

$$\tilde{\rho} = \frac{\rho}{\rho_0} \tag{25}$$

$$\tilde{v} = \frac{v}{u_0}. \tag{26}$$

Normalized quantities:

$$\hat{R} = R \frac{L}{K} \tag{27}$$

$$\hat{L} = L \frac{U}{K} \tag{28}$$

$$\hat{G} = G(ZK) \tag{29}$$

$$\hat{C} = (UK) \tag{30}$$

$$\hat{\Re} = \frac{e \rho_0 T^2}{m_e \varepsilon_0} \Re = \omega_p^2 T^2 \Re \tag{31}$$

Derivatives with respect to z and then ψ become

$$\frac{\partial}{\partial z} = \frac{1}{L} \frac{\partial}{\partial \hat{z}} \tag{32}$$

$$\frac{\partial}{\partial \psi} = \frac{1}{\omega_0 T} \frac{\partial}{\partial \hat{\psi}} \tag{33}$$

Some other relationships between DC parameters can be written as follows:

$$\mathbb{C} = \left(\frac{K I_0}{4 V_0} \right)^{1/3} \tag{34}$$

$$I_0 = \rho_0 u_0 A \tag{35}$$

$$u_0 = \left(\frac{2 e V_0}{m_e} \right)^{1/2} \tag{36}$$

In Eqs. (34)–(36), ρ_0 is the DC linear charge density, V_0 is the DC beam voltage, I_0 is the DC beam current, and $\mathbb{C}$ is the Pierce gain parameter.

The function $x(z, \psi)$ is the Fourier series relations that is defined as follows [3, 4, 16]

$$x(z, \psi) = \sum_{j=-\infty}^{\infty} \tilde{x}_j(z) e^{i f_j \psi} \tag{37}$$

$$\tilde{x}_j(z) = \frac{1}{2\pi} \int_{2\pi} x(z, \psi) e^{-i f_j \psi} \mathrm{d}\psi \tag{38}$$

where,

$$f_j = (m f_1 \pm n f_2) \tag{39}$$

f_j is the set of frequencies that are the drive frequencies together with the frequencies produced from nonlinear interactions, m and n are the integers positive and negative, and ψ is the periodic function.

(z, ψ) are Eulerian independent variables and (z, ψ_0) are Lagrangian independent variables, where z is axial position and ψ is phase, and ψ_0 is the phase position of a fluid element with respect to the stream wave. The transformation from Lagrangian to Eulerian coordinates is given by functions Z and ψ

$$\begin{bmatrix} z \\ \psi \end{bmatrix} = \begin{bmatrix} Z(z, \psi_0) \\ \Psi(z, \psi_0) \end{bmatrix} \tag{40}$$

$Z(z, \psi_0)$ is the axial position of fluid element ψ_0 at z so

$$Z(z, \psi_0) = z. \tag{41}$$

A function g_E of Eulerian variables (z, ψ) is transformed to a function g_L of Lagrangian variables (z, ψ_0) using

$$g_L(z, \psi_0) = g_E(Z(z, \psi_0), \Psi(z, \psi_0)) \tag{42}$$

According to Eqs. (40) and (41), transformation matrix of equation is as follows:

$$\begin{bmatrix} 1 & 0 \\ \dfrac{\partial \Psi}{\partial \psi} & \dfrac{\partial \Psi}{\partial \psi_0} \end{bmatrix} \tag{43}$$

That Jacobin matrix equals to:

$$J = \frac{\partial \Psi}{\partial \psi_0} \tag{44}$$

The partial derivatives are transformed as follows

$$\begin{bmatrix} \dfrac{\partial}{\partial z} & \dfrac{\partial}{\partial \psi} \end{bmatrix} = \begin{bmatrix} \dfrac{\partial}{\partial z} & \dfrac{\partial}{\partial \psi_0} \end{bmatrix} \begin{bmatrix} 1 & 0 \\ \dfrac{\partial \Psi}{\partial z} & \dfrac{\partial \Psi}{\partial \psi_0} \end{bmatrix}^{-1} \tag{45}$$

According to a certain method in the Lagrangian model, we have:

$$\frac{\partial \Psi}{\partial z} = \frac{\omega_0}{u_0}\left(1 - \frac{u_0}{v_L}\right) \tag{46}$$

Using Eq. (46), convective derivative in the Eulerian coordinates becomes

$$v_{\mathrm{E}}\frac{\partial v_{\mathrm{E}}}{\partial z} + \omega_0\left(\frac{v_{\mathrm{E}}}{u_0} - 1\right)\frac{\partial v_{\mathrm{E}}}{\partial \psi} = v_L\frac{\partial v_L}{\partial z} \tag{47}$$

Applying derivative transformation relation (45) to the continuity Eq. (15), the following relation is obtained:

$$\frac{\partial \Psi}{\partial \psi_0}\frac{\partial \rho_L v_L}{\partial z} = -\omega_0\frac{\partial \rho_L}{\partial v_L}\frac{\partial v_L}{\partial \psi_0} \tag{48}$$

Derivative from Eq. (46) relative to ψ_0 one gets

$$\frac{\partial}{\partial z}\frac{\partial \Psi}{\partial \psi_0} = \frac{\omega_0}{(v_L)^2}\frac{\partial v_L}{\partial \psi_0} \tag{49}$$

Substitute (49) into (48) and integrate to get

$$\frac{\partial \Psi}{\partial \psi_0}\rho_L v_L = \kappa \tag{50}$$

In which κ is a constant of integration. By definition $\Psi(0,\psi_0) = \psi_0$, the values $\frac{\partial \Psi}{\partial \psi_0}$ and $\rho_L v_L$ on the ψ_0 axis, are $\frac{\partial \Psi(0,\psi_0)}{\partial \psi_0} = 1$ and $\rho_0 v_0$, respectively. Considering the following equation

$$\rho_0(0,\psi_0)v_0(0,\psi_0) = \frac{I_0(0,\psi_0)}{A} \tag{51}$$

Equation (50) becomes

$$\left|\frac{\partial \Psi}{\partial \psi_0}\right|\rho_L(0,\psi_0)v_L(0,\psi_0) = \kappa = \frac{I_0(\psi_0)}{A} \tag{52}$$

The Fourier coefficient of ρ_E is expressed as

$$\tilde{\rho}_{\mathrm{E}}^l = \frac{1}{2\pi}\int\limits_{2\pi} \rho_{\mathrm{E}}e^{-if_i\psi}\mathrm{d}\psi \tag{53}$$

Pulling Eq. (53) back to Lagrangian coordinates (for fixed z) and using Eq. (44) one gets

$$\begin{aligned}
\tilde{\rho}_{\mathrm{E}}^l &= \frac{1}{2\pi}\int\limits_{2\pi} \rho_{\mathrm{L}}\left|\frac{\partial \Psi}{\partial \psi_0}\right|e^{-if_i\Psi(0,\psi_0)}\mathrm{d}\psi_0 \\
&= \frac{1}{2\pi}\int\limits_{} \frac{I_0(0,\psi_0)}{Av_L(0,\psi_0)}\left|\frac{\partial \Psi}{\partial \psi_0}\right|e^{-if_i\Psi(0,\psi_0)}\mathrm{d}\psi_0
\end{aligned} \tag{54}$$

Using Eqs. (37), (38) and (54), the circuit equations, space charge equation, Newton's law and phase relation (11–15), in Lagrangian coordinates, the following equations are created

$$\frac{\mathrm{d}\tilde{V}_j}{\mathrm{d}z} = -\frac{if_j\omega_0}{u_0}\tilde{V}_j - \frac{if_j\omega_0\tilde{K}(f_j\omega_0)}{\tilde{v}_{\mathrm{ph}}(f_j\omega_0)}\tilde{I}_j \tag{55}$$

$$\begin{aligned}
\frac{\mathrm{d}\tilde{I}_j}{\mathrm{d}z} &= -\frac{if_j\omega_0}{\tilde{K}(f_j\omega_0)\tilde{v}_{\mathrm{ph}}(f_j\omega_0)}\tilde{V}_j - \frac{if_j\omega_0}{u_0}\tilde{I}_j \\
&\quad + if_j\omega_0\frac{1}{2\pi}\int\limits_{2\pi}\frac{I_0(\psi_0)}{v(z,\psi_0)}e^{-if_j\Psi(z,\psi_0)}\mathrm{d}\psi_0
\end{aligned} \tag{56}$$

$$\frac{\mathrm{d}\tilde{E}_j}{\mathrm{d}z} = -\frac{if_j\omega_0}{u_0}\tilde{E}_j + \frac{1}{\varepsilon_0 A}\frac{1}{2\pi}\int\limits_{2\pi}\frac{I_0(\psi_0)}{v(z,\psi_0)}e^{-if_j\Psi(z,\psi_0)}\mathrm{d}\psi_0 \tag{57}$$

$$\frac{\partial v}{\partial z} = \frac{1}{v}\sum_{-\infty}^{+\infty}\left\{\frac{if_j\omega_0 e\tilde{K}(f_j\omega_0)}{m_e\tilde{v}_{\mathrm{ph}}(f_j\omega_0)}\tilde{I}_j + \frac{e}{m_e}\Re(f_j\omega_0)\tilde{E}_j\right\}e^{if_j\Psi(z,\psi_0)} \tag{58}$$

$$\frac{\partial \Psi}{\partial z} = \frac{\omega_0}{u_0}\left(1 - \frac{u_0}{v}\right) \tag{59}$$

where $-\infty < j < \infty$, and $f_j = f_m + f_n$, for $m > n$, $f_m > f_n$.

For practical implementation, one neglects higher frequencies and limits to $-M < j < M$.

The equations in (55–59) are ordinary differential equations, and we will use standard ordinary differential equation integration techniques. The problem is an initial value problem, where one can calculate the proper initial values using (38). Otherwise for, $j \neq 0$, $\tilde{E}_j = \tilde{v}_j = \tilde{\rho}_j = 0$, also for $j = 0$, $\tilde{E}_0 = \tilde{V}_0 = \tilde{I}_0 = 0$ and $\tilde{v}_0(0) = u_0$, $\tilde{\rho}_0(0) = \rho_0$.

In addition to the initial conditions mentioned above, there are other parameters that are very important in the performance of the TWT. These constant values are given in Table 1.

Numerical results

In this work, different voltages have been applied to the electron beam in the assumed frequency range in order to evaluate the TWT response. In this process among different mathematical models, the Lagrangian mathematical model

Table 1 Constant values

Parameter	Value	Parameter	Value	Parameter	Value
Electron mass (m_e)	9.11×10^{-31} kg	Circuit length (L)	0.42 m	Number of circuit sections	10
Electron charge (e)	1.6×10^{-19} c	Beam outer radius	0.0009652 m	Number dispersion frequency	27
Helix radius	0.002353 m	Beam inner radius	0.0		
Helix wire width (w)	0.000305 m	Beam current (I_0)	0.0655 A	Base frequency (ω_0)	1 GHz

has been applied on the TWT, which includes all the nonlinear features of a TWT properly. Accordingly, the governing equations on TWTs which indicate the changes in voltage and current circuit, space charge field as well as velocity and density of the electron beam are written. Also by applying the initial conditions appropriate to the TWT features and using fixed step fourth-order Runge–Kutta integrator numerical method, the differential equation systems 55–59 have been solved.

In this study, the TWT has been examined in two different situations; as a result, two different responses are reached which are discussed below:

Situation (1)

In this case, the response of the TWT is examined under the influence of applying the voltage in the absence of harmonic and intermodulation frequencies (single-tone mode). In this situation, the operation of the TWT was studied in the single frequency mode, which means the output frequency from the TWT is the same as the single input frequency entered to it. The final results of the calculations in this mode are revealed in diagrams 2–3 which display output power in terms of distance (z), voltage (v) and frequency (f).

In Fig. 2, the output power of the circuit is plotted at frequencies of 1400, 1600 and 1800 MHz, in terms of different voltage of the electron beam. In this case, the circuit power is calculated for each single input frequency, the harmonic frequencies and the intermodulation are not
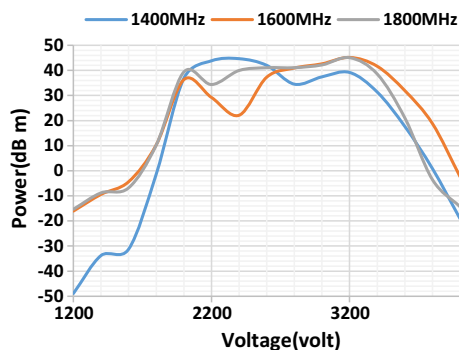
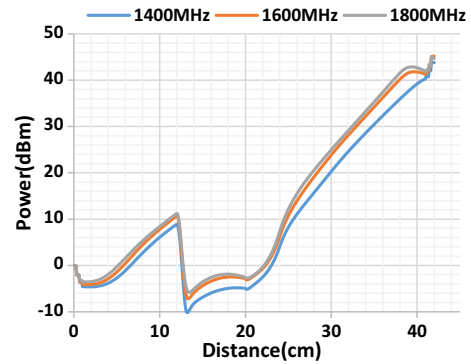**Fig. 2** Circuit output power versus of the electron beam voltages

Fig. 3 Circuit output power versus of the axial distance, $V = 3200$ v

produced. In the voltage range of 2000–3300 v, the amplification of the wave at these three frequencies is approximately constant.

In Fig. 3, the output power is plotted in terms of axial distance, for a voltage of 3200 v at frequencies of 1400, 1600 and 1800 MHz. It is noticeable that the circuit power is saturated at 40 cm in all the three frequencies. According to Fig. 2, if the voltage of 2600 was selected, the amplification of all the three frequencies would occur alike.

Situation (2)

In this case, the response of the TWT is examined under the influence of applying the voltage in the presence of drive, harmonic and intermodulation frequencies (multi tone mode). Here, when two input frequencies which their difference is about 1 MHz are entered to the TWT, drive frequencies as well as unwanted harmonic and intermodulation output frequencies are produced (Table 2). The final results of the calculations in this mode are revealed in diagrams 4–8 which display output power in terms of distance (z), voltage (v) and frequency (f).

In Fig. 4, the output power of the circuit is plotted at frequencies of 1400, 1600 and 1800 MHz, in terms of different voltage of the electron beam. In this case, the two main input frequencies are considered (Table 2); as a result, harmonic and intermodulation frequencies are produced. In the voltage range of 2000–2800 v, the difference in amplification of the wave at these three frequencies is small (Fig. 5).

Table 2 Nonlinear second- and third-order products created for two input signals

Input frequency (MHz)	Frequencies generated by the TWT (MHz)			
Driven-order	First-order	Second-order harmonics	Third-order	
			Harmonics	Intermodulation
1400, 1401	1400, 1401	1, 2800, 2801, 2802	4200, 4203	1399, 1402, 4201, 4202
1600, 1601	1600,1601	1, 3200, 3201, 3202	4800, 4803	1599, 1602, 4801, 4802
1800, 1801	1800,1801	1, 3600, 3601, 3602	5400, 5403	1799, 1802, 5401, 5402

Fig. 4 Circuit output power versus of the electron beam voltages
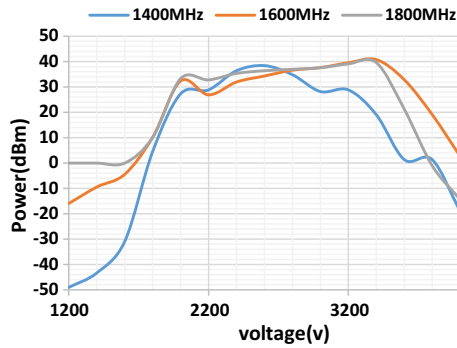
Fig. 6 Circuit output power versus axial distance, $V = 3200$ v

In the above figure, the output power is plotted in terms of axial distance, for a voltage of 3200 v at frequencies of 1400, 1600 and 1800 MHz. These calculations are done for each of the three frequencies in the presence of second-order harmonic and intermodulation frequencies (table). It is noticeable that the circuit power is saturated at 38 cm at all three frequencies.

In Fig. 6, the output power is plotted in terms of axial distance, for a voltage of 3200 v at frequencies of 2800, 3200 and 3600 MHz. These frequencies are second-order harmonics, which are produced by the nonlinear response of the pipe to the two main input frequencies, as shown in Table 2. As shown in Fig. 6, at these frequencies, the saturation occurs with a gentle slope.

In Fig. 7, the output power of the circuit is plotted at frequencies of 2800, 3200 and 3600 MHz, in terms of different voltage of the electron beam. These frequencies are second-order harmonics (Table 2). In the range of
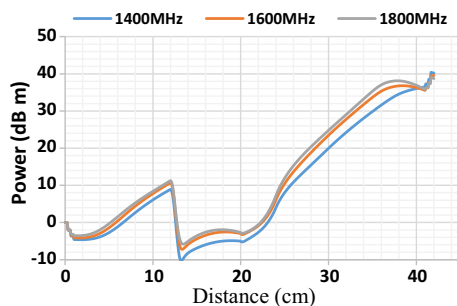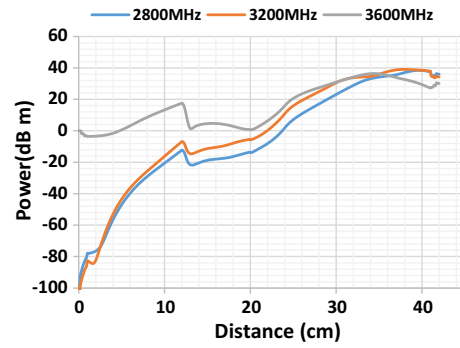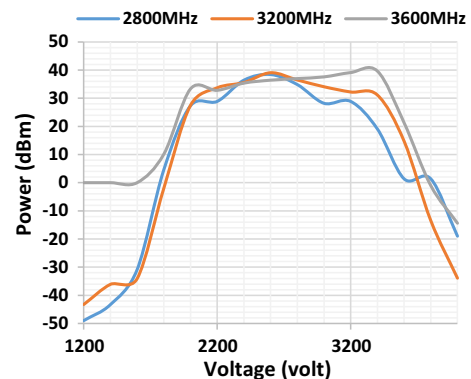

Fig. 7 Circuit output power versus beam voltage

2000–2600 v, it is clear that the output power difference in the circuit is small in these three frequencies.

In Fig. 8, the output power of the circuit is plotted in terms of different voltage of the electron beam, at frequencies of 1399, 1599 and 1799 MHz. These frequencies are third-order intermodulation frequencies (Table 2). In the range of 2200–3000 v in all the three frequencies, the output power difference in the circuit is small.

Discussion and conclusion

As it can be seen, when voltage changes at different frequencies in TWT, the output power will change. Voltage variation is important in a particular range.
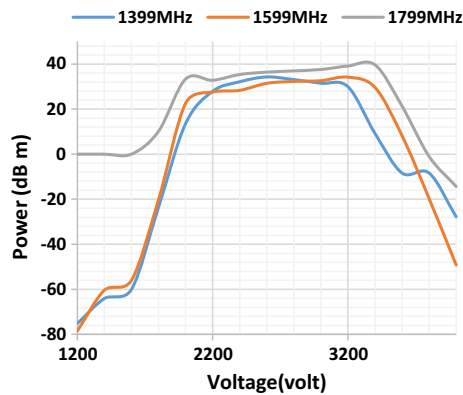

Fig. 5 Circuit output power versus axial distance in, $V = 3200$ v

Fig. 8 Circuit output power versus beam voltage

Applying a lower voltage is needed to achieve a higher power in low frequencies, but for gaining a higher power in high frequencies, using a bigger voltage is required. In a specified voltage range, the changes in the output power are not noticeable. Beam emission voltage has a direct relationship with output power to a certain extent, but after a certain limit this relationship becomes inverse which means increasing beam emission voltage results in the decrease in output power. This happens because of the saturation phenomena which is the nonlinear operation of TWT. In smaller frequencies, saturation phenomena (this phenomena happens when increasing of the output power stops) in the TWT happen in lower voltage. For instance in Fig. 2, it can be seen that the blue plot (1400 MHz) decreases in a lower voltage (about 3200 v), but the orange plot (1600 MHz) along with the gray plot (1800 MHz) decreases in a higher frequency (about 3400 v) but with different slopes. Comparing Figs. 2 and 3, it is observed that at 1400 MHz (single-tone mode), for a voltage of 2200 V, the TWT output power is 45 dBm, while this power is 30 dBm in the same conditions in a multi tone mode. All shapes show the fact that the voltage applied at each frequency does not create a unique power; at some voltages, the power generated at various frequencies is the same approximately.

References

1. Pierce, J.R.: Traveling Wave Tubes, pp. 3–10. D Van Nostrand, New York (1950)
2. Rowe, J.E.: Nonlinear Electron-Wave Interaction Phenomena, pp. 3–10. Academic Press Inc, New York (1965)
3. Wöhlbier, J.G., Booske, J., Dobson, I.: The multi-frequency spectral Eulerian (Muse) model of a traveling-wave tube. IEEE Trans. Plasma Sci. **30**, 1063–1075 (2002)
4. Wöhlbier, J.G.: Nonlinear distortion and suppression in traveling wave tubes: insights and methods. Doctor of Philosophy's thesis, University of Wisconsin-Madison, pp. 10–22 (2003)
5. Joo, Y.D., Sinha, A.K., Park, G.S.: Simple nonlinear analysis code for helix traveling wave tube. In: Vacuum Electronics Conference, pp. 118–119 (2004)
6. Srivastava, V., Joshi, S.N.: One-dimensional nonlinear model for helix TWTs. IETE Tech. Rev. **6**, 500–507 (1989)
7. Singh, A., John Scharer, E., Booske, J., Wöhlbier, J.G.: Second- and third-order signal predistortion for nonlinear distortion suppression in a TWT. IEEE Trans. Electron Devices **52**, 709–717 (2005)
8. Males-iliac, N., Budimir, D., Milovanovic, B.: Improved linearization technique that uses injection of second harmonics. Microw. Opt. Technol. Lett. **38**, 150–153 (2003)
9. Srivastava, V., Joshi, S.N.: Improved nonlinear model for multi-signal analysis of helix TWTs. IEE Proc. **139**(2), 129–134 (1992)
10. Joo, Y.-D., Sinha, A.K., Wei, Y., Park, G.-S.: Simplified approach to the nonlinear analysis in helix slow-wave-structure for a traveling wave tube. Jpn. J. Appl. Phys. **42**, 7104–7111 (2003)
11. Wohlbier, J.G., Dobson, I., Booske, J.H.: On the physics of harmonic injection in a traveling wave tube. IEEE Trans. Plasma Sci. **32**(3), 1073–1085 (2004)
12. Singh A.: Experimental investigation of TWT nonlinearities and distortion suppression by signal injection. A thesis for the degree of Master of Science 2003, University of Wisconsin—Madison
13. Srivastava, V., Joshi, S.N., Ravinder, B., Carter, R.G., Sinha, A.K.: Design of helix slow-wave structures for high efficiency TWTs. IEEE Trans. Electron Devices **47**(12), 2438–2443 (2000)
14. Wöhlbier, J.G., Booske, J.: Mechanisms for phase distortion in a traveling wave tube. Phys. Rev. E **69**, 066502 (2004)
15. Joo, Y.D., Park, G.S.: Development of a simplied one-dimensional nonlinear helix traveling wave tube code based on the lagrangian disk model. IEEE Trans. Electron Devices **48**(1), 3–11 (2001)
16. Sheykhe, F., Saviz, S., Salem, M.: Comparison of the effect of annular and solid electron beams on linear and nonlinear traveling wave tube. Results Phys. **7**, 4324–4331 (2017)